Available online at www.elixirpublishers.com (Elixir International Journal)

Chemical Physics

Elixir Chem. Phys. 53 (2012) 11922-11927

ISSN: 2229-712X

The influence of Al doping on optical, electrical and structural properties of transparent and conducting SnO_2 : Al thin films prepared by spray pyrolysis technique

Maxwell Mageto[1] and M. Mwamburi[2]

[1]Department of Physics, Masinde Muliro University of Science and Technology, P.O. Box 190, 50100 Kakamega, Kenya.

[2]Department of Physics, Moi University, P.O. Box 1125, Eldoret, Kenya.

ARTICLE INFO

Article history:

Received: 25 October 2012;

Received in revised form:

20 November 2012;

Accepted: 6 December 2012;

Keywords

Spray Pyrolysis,

Tin Oxide,

Transparent conductors,

Doping.

ABSTRACT

The influence of increasing Al concentration on the electrical, optical and structural properties of transparent and conducting SnO_2 : Al films has been investigated. The films were deposited on glass substrates at a temperature of 480°C using a hydro-alcoholic solution consisting of $SnCl_4.5H_2O$ and $AlCl_3.6H_2O$ with various Al-doping levels from 0 to 0.53 being spray ratios of $AlCl_3$: SnO_2 in solution. The effect of changing the aluminum-to-tin spray ratio, [Al]/[Sn], from 0 to 0.53 was investigated. The optical properties were studied in the UV/VIS/NIR region. The optical band gap for undoped SnO_2 films lay at 3.9 eV, whereas for high Al -doped films it shifts towards lower energies in the range of 3.9 – 3.61 eV. The results of x-ray diffraction have shown that the deposited films are polycrystalline without any second phases with preferential orientations along the (110), (101), (200) and (211) planes and an average grain size of 25.7 nm. It has been shown that increasing Al doping concentration lowers both the grain size and electrical conductivity of tin oxide significantly.

Introduction

Doped SnO_2 is besides doped In_2O_3 and ZnO the best known representative of the class of transparent electrical conductors and finds use in form of poly-crystalline thin films [1-4, 11]. Its applications include photovoltaic and electro-chromic devices, glass coatings for furnace windows, for deicing or defogging as well as transparent electrodes for liquid crystal displays and as a gas sensor. Metal-oxides often behave like semiconductors with a wide band gap due to their strong chemical bonds [1-4, 11].

SnO_2 Thin films can be prepared by a number of methods, such as CVD [22], sputtering [23], spray pyrolysis [24], plasma and sol–gel methods [25], each of which has advantages and disadvantages. Spray pyrolysis is suitable for substrates with complex geometry, and can be used for a variety of oxide materials. The advantages of spray pyrolysis include [10]: it can be easy and cheap since it is a non-vacuum process; substrates with complex geometries can be coated; leads to uniform and high quality coatings, low crystallization temperatures and porosity can be easily tailored. The pyrolytic spray technique is the most suitable when high visible transmission and high infra-red reflectance are desired [1]. In spray pyrolysis the precursor solution is pulverised as a fine mist via a spray nozzle and a carrier gas at high pressure. The so produced mist condenses on a preheated substrate, and is instantly pyrolysed. The process can be conducted in one or more pulses to obtain uniform films.

To reduce its resistivity, SnO_2 can be doped with either fluorine or Antimony[1, 11-12] . In this case F^{-1} substitutes O^{-2} and Sb^{5+} substitutes Sn^{4+} therefore each acts as an electron donor resulting in a conduction mechanism of the n-type. The reason why undoped SnO_2 can be infra-red reflecting i.e conducting, is that doping occurs from the chlorine in the spray solution and also intrinsically from oxygen vacancies[1]. Annealing of the films in air results in a reduction in conductivity due to the fact that there is a corresponding reduction in the degree of intrinsic doping [1].

In this report we present reflectance, transmittance and resistivity measurements on SnO_2 : Al films on glass substrates prepared by the pyrolytic spray method with varying Al dopant concentration. The aim was to fabricate and characterize a p-type semiconductor. The ionic radii of Al^{3+} is 0.5 Å and its electronegativity is 1.5. This is near from those of Sn^{4+} (0.71 Å and 1.96)[13]. Thus, Al is supposed to be substituted to Sn, in the lattice making a p-type semiconductor. Currently there is a large amount of enthusiasm in the search for a p-type transparent conducting oxide (TCO). The photovoltaic industry can benefit from the development of a p-type TCO since greater flexibility in cell design by using p-type TCOs can be exploited to increase the cell efficiencies. For instance, using a combination of n- and p-type TCO materials, cells can be stacked to increase efficiency. Another opportunity for p-type TCO applications are as functional windows, which act as windows while at the same time producing electricity. As alternative sources of energy become more crucial in the future, functional windows may be an important technological advancement.

Tele:

E-mail addresses: jmmageto@yahoo.com

Transparent transistors are another possible application based on the development of a p-type TCO.

Experimental

Sample preparation

Undoped and Aluminum-doped tin oxide films were pyrolytically deposited onto 1mm thick $2.5\times 7\,cm^2$ glass substrates by spray pyrolysis. The detailed description of the spray pyrolysis reactor and the optimization of the film growth is given elsewhere [1]. The heterogeneous reaction involved in the film formation is [2, 3]

$$SnCl_4 + 2\ H_2O \Rightarrow SnO_2 + 4HCl \qquad \text{Eq. 1}$$

but according to Ref [3] if the reaction is completed then the resulting film would become an insulator. Since the films obtained by pyrolytic decomposition are conducting, the expected reactions are

$$2SnCl_4 + 4\ H_2O \Rightarrow SnO_2 + SnO + 7HCl + \tfrac{1}{2}O_2 + \tfrac{1}{2}Cl_2 + \tfrac{1}{2}H_2 + e \qquad \text{Eq. 1b}$$

$$2\ SnCl_4\ +\ 4\ H_2O \Rightarrow SnO_2 + SnO + 8HCl + \tfrac{1}{2}O_2 + \tfrac{1}{2}H_2 + 2\ e \qquad \text{Eq. 1c}$$

The $SnO_2:Al$ films were produced from 2.0 M solution of hydrous tin chloride ($SnCl_4.5H_2O$) in ethanol and a few milliliters of hydrochloric acid and a 1.5 M aqueous dopant solution of hydrous aluminium chloride ($AlCl_3.6H_2O$). A separate spray nozzle was used for the dopant solution.

The doping concentration was varied by a carrier-gas flow rate ratio of x : 5 for $AlCl_3.6H_2O$ to $SnCl_4.5H_2O$ solutions, where ($x = 0.00,\ 1.00,\ 1.36,\ 1.60,\ 2.00,\ 2.65$) i.e. Variation in doping concentration was achieved by increasing the $AlCl_3.6H_2O$ flow rate. Compressed air was used as the carrier gas. For the different samples, the substrate temperature was maintained at $480^{\circ}C$.which is known to be the optimum temperature for formation of tin oxide films [4]. The spray pyrolysis technique is a typical method that has been used for the deposition of materials in thin form. The deposition apparatus consists of a spray chamber, hot plate, two spray nozzles and two input gas valves.

Sample characterization

The transmittance and reflectance measurements were done at near normal incidence in the solar wavelength range from 0.3 to 2.5 μm on a Perkin-Elmer Lamda 900 UV/VIS/NIR double beam spectrophotometer equipped with an integrating sphere. The reflectance measurements in the far infrared were done in the wavelength range 2.5 to 50 μm using FTIR spectrophotometer. Thickness of the as-deposited samples prepared with different Al doping concentrations were calculated using the modified envelope method [5-7]. The film thickness is given by

$$t = \frac{\lambda_1\lambda_2}{2(\lambda_1 n_2 - \lambda_2 n_1)} \qquad \text{Eq. 2}$$

Where λ_1 and λ_1 are the wavelengths at which two successive maxima or minima occur and n_1 and n_2 are the corresponding refractive indices or

$$t = \frac{\lambda_1\lambda_2}{4(\lambda_1 n_2 - \lambda_2 n_1)} \qquad \text{Eq. 2b}$$

Where λ_1 and λ_1 are the wavelengths at which two successive maxima and minima occur and n_1 and n_2 are the corresponding refractive indices [6,7]. The estimated thickness was verified by fitting the experimental spectral data to theoretical spectral data in the wavelength range 0.3 - 2.5 μm and also from the SEM cross sections.

The structural properties were determined using a Siemens D5000 X-ray diffractometer (XRD). The glazing incident angle was 1^0 in parallel beam geometry with the diffraction angle, 2θ, between 20^0 and 70^0. The wavelength, λ, of the CuK_α radiation was 1.540598 Å. The effective grain size was determined from the full-width at half-maximum (FWHM) of the x-ray peaks line of the (110) plane using the Scherer formula (equation 3) and the Williamson–Hall formula (equation 4):

$$FWHM = \frac{0.9.\lambda}{L.\cos(\theta)} \qquad \text{Eq. 3}$$

The information on strain (ε) and the grain size (L) of the deposited films have been obtained from the following relation [9]

$$\frac{\beta\cos\theta}{\lambda} = \frac{1}{L} + \frac{\varepsilon\sin\theta}{\lambda} \qquad \text{Eq. 4}$$

Where β is the FWHM.

A high resolution LEO 1550 SEM with a field emission gun was used to examine grain size , surface and cross-sectional morphologies of different concentrations Al in the doped samples on silicon substrates. The cross sections were created by breaking the sample into two pieces.

The sheet resistance of the thin films was determined by the four-point probes technique, which used In tips in a linear arrangement and touched closely the coated surface. By measuring the sheet resistance (R_s) and the average thickness, t, of the films, the electrical resistivity, ρ (or conductivity, σ) of the samples was calculated using the following relation [4]:

$$\rho = \frac{1}{\sigma} = R_s\ \ t \qquad \text{Eq. 5}$$

The hot point probe was used as a quick method to determine if the thin film is n-type or p-type [8]. The setup requires a heated probe and an unheated probe connected to an ammeter. The two probes are placed on the sample surface. Carriers near the hot probe gain thermal energy from the heat and move away from the hot probe, leaving a net charge near the probe. For a p-type material, negative charge exists near the hot probe. For an n-type material, the charge is positive. This charge separation results in a voltage and thus a current, which is detected by the ammeter. The sign of the current indicates whether the semiconductor is n-type or p-type [8].

Results and Discussion

Structural Properties

Figure 1 shows the XRD patterns of the undoped and Al doped tin oxide films on glass substrates. The peaks in the spectra are identified as originating from reflections from the (110), (101), (200) (211) planes of polycrystalline cassiterite structure tin oxide. No peaks from starting materials or any residual species were found in the spectra, confirming the proper phase formation of the materials [14]. It is clear that Al substitutes for Sn in the SnO_2 lattice since the crystal structure is not distorted. The doping spray ratio of $Al:Sn$ was in the range 0 % - 53%. No change of the position of the XRD peaks with the Al doping for the above percentages was observed and hence it was not alloying[14,15,16]. In addition, no extra peak appeared in the XRD pattern for the Al incorporated in the films hence

any possibility of phase separation was also ruled out [15]. XRD pattern did not present any shift in lattice parameters with increasing Al doping concentration, suggesting that Al solubility in SnO_2 was low [27]

Figure 3 shows that Al doping lowers the grain size. The effect of Al doping on SnO_2 has been investigated by various researchers in the past and it was reported as a grain growth inhibitor [14,15]. With increasing Al dopant in the tin oxide film, the crystallinity of SnO_2 decreased [14,15].

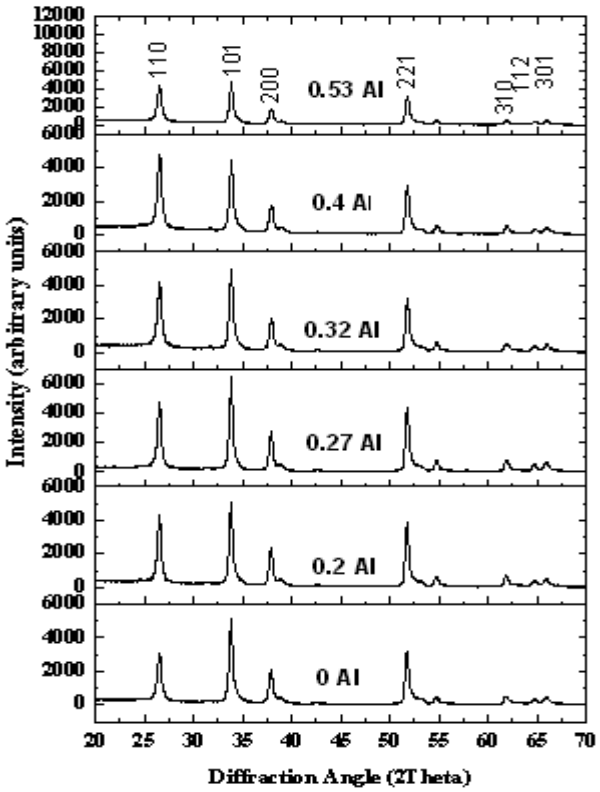

Fig 1: XRD pattern of undoped and Al-doped SnO_2 films deposited on glass substrates at 480^{0}C

From Figure 2, the slope of the graph $\beta\cos(\theta)/\lambda$ versus $\sin(\theta)/\lambda$ depicts the strain as being (0.022 – 0.041) nm compared to the literature value 0.0135 for sparayed

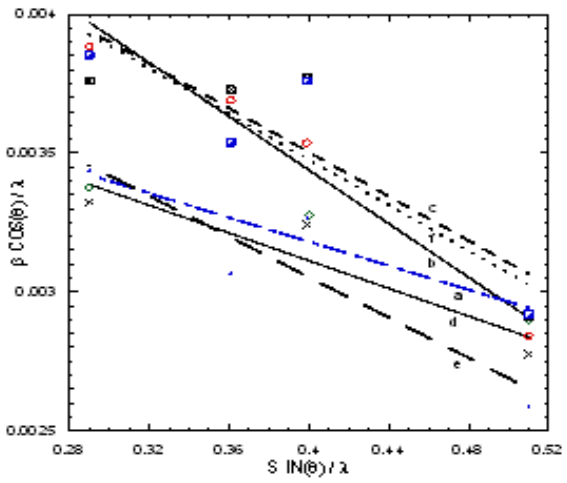

Fig.2. A graph $\beta\cos(\theta)/\lambda$ versus $\sin(\theta)/\lambda$

SnO_2 films [16], and the intercept on y-axis gives the crystallite size of (18.61 – 24.66) nm for the 53% Al doped SnO_2 and undoped SnO_2 respectively while from Scherer formula grain size is in the range (21.6 – 25.8)nm compared to the literature value of 25nm for undoped tin oxide.

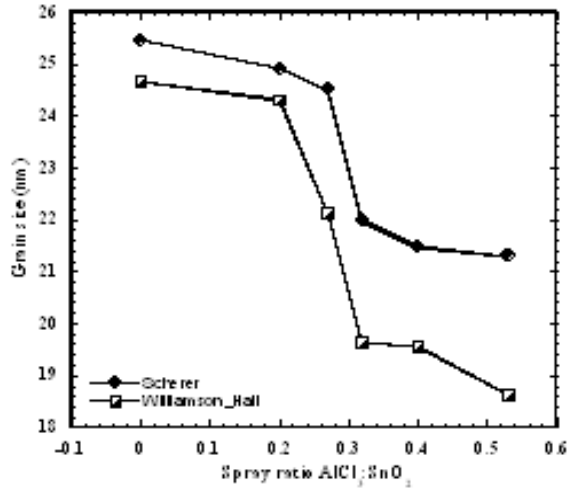

Fig. 3 Variation of grain size with doping concentration

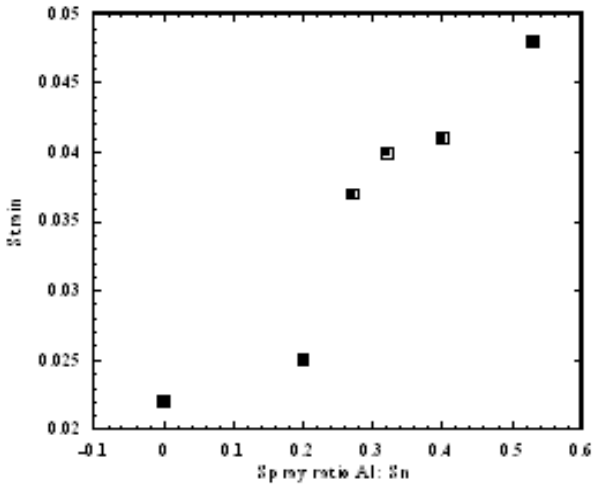

Fig. 4 Strain Versus doping concentration

The crystallite size of SnO_2 was decreased with increasing Al concentration. Hence Al is a grain growth inhibitor. The strain increased with increasing Al concentration in the films as shown in Figure 4.

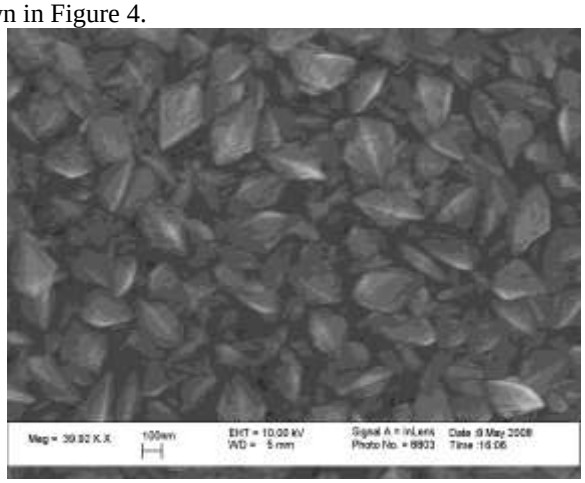

Fig. 5. SEM image of (a) undoped SnO_2

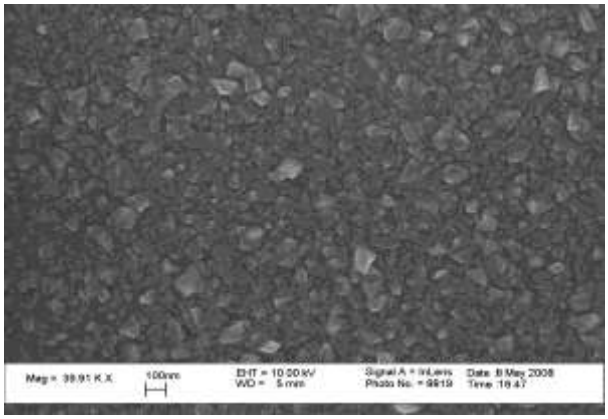

(b) 53% Al doped SnO_2

From the SEM observations in Fig. 5, it can be concluded that the average particle size of undoped tin oxide is 70-150 nm. The particle size is smaller in Al-containing samples and the size homogeneity is poorer. These effects can be considered as a consequence of the isomorphic substitution of Sn(IV) by Al-(III), as shown by Al MAS NMR in Ref [26], which induces some lattice distortions as the size of the Sn and Al ions differs significantly (0.71 and 0.50 Å, respectively) [13,26], avoiding large particle sizes.

Electrical Studies

To evaluate the Al solubility in SnO_2 lattice, the variation of the electrical resistance with the Al doping concentration was measured. Figure 6 shows the variations of resistivity with increasing dopant concentration in $SnO_2:Al$ films. Earlier studies on Al doping on SnO_2 have shown an increased resistance on doping with Al [14]. Mohagheghi et al. [4] reported that the electrical resistance increases with resistance up to a certain optimum level of Al doping beyond which the resistance drops before increasing again. Our results show that resistivity of SnO_2 increases with Al doping. Undoped film has some conductivity probably due to oxygen vacancies. Since Al^{3+} replaces some of the Sn^{4+} sites, there is a net decrease in charge carrier concentration. Each gives an electron to the conduction band, conductivity decreases because Al has one electron less than Sn and thus compensates these conduction band electrons. We can assume that each Al introduced in the lattice of SnO_2 traps a conduction electron. This can be explained as follows;

The conduction band (CB) of tin oxide semiconductor is derived mainly from metal (Sn^{4+}) orbitals. When a metal dopant (Al^{3+}) is used, it is electrically active when it substitutes for the primary metal (Sn). The CB thus receives a strong perturbation from each metal dopant, the scattering of conduction electrons is enhanced and the mobility and conductivity are decreased [21]. In contrast, when e.g F substitues for O, the electronic perturbation is largely confined to the filled valence band (VB) and the scattering of conduction electrons is minimized.

Optical studies

In order to compare the transparency of $SnO_2:Al$ thin films with various Al-doping levels, samples were selected and their optical spectra in the UV-VIS–NIR region and far infrared region were measured. The optical transparency of $SnO_2:Al$ thin films for various Al-doping levels is shown in figure 1. As shown in Fig. 1, prior to the band edge near 540 nm, the film exhibits a transparency near 83% (for undoped) to 87 % for the heavily Al-doped tin oxide. The transparency at 540 nm increased with increasing Al doping concentration as seen in figure 7 (a). Near the infrared wavelength range, the transparency increase with Al doping became more pronounced. In the far infrared wavelength range, the reflectance decreases with increasing Al doping concentration as evidenced in figure 7 (b).

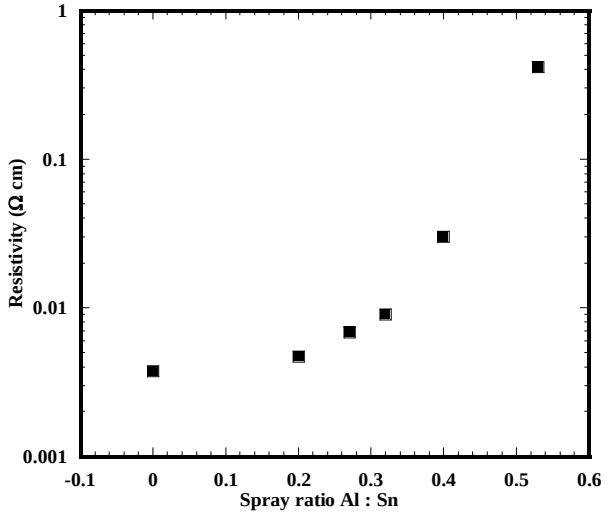

Fig. 6 Variation in electrical resistivity with increasing Al doping concentration in tin oxide

For the optical bandgap measurement, films were deposited on quartz substrates and their transmission, T and reflectance, R spectra were recorded. Next, the optical absorption coefficient, α for different wavelengths, λ was determined from the expression [18]

$$\alpha(\lambda) = \frac{1}{t} \ln\left(\frac{1-R(\lambda)}{T(\lambda)}\right) \qquad \text{Eq. 6}$$

Where t is the film thickness. For direct transitions the absorption coefficient varies as $(hv - E_g)^{\frac{1}{2}}$ [19] where E_g is the direct band gap. Figure 8 shows plots of $(\alpha hv)^2$ versus photon energy, hv, in the high absorption region. Extrapolation of the curve to $hv = 0$ gives the direct band gap.

The calculated direct bandgap values of $SnO_2:Al$ films lay in the range 3.86 eV to 3.99 eV for the 53% Al doped and undoped SnO_2 respectively; which are also comparable with the values already reported; 3.604 to 4.105 eV [16] 3.87 to 4.21 eV [15]. The bandgap slightly narrows down due to the decrease in the number of charge carriers with increase in Al-doping.

The optical constants are reported in Figure 9 showing spectral refractive index n (λ) and extinction coefficient k (λ) for undoped and doped films. The 32 to 53% Al doped SnO_2 film exhibit a less conducting behavior compared to the undoped, 20% Al doped and 27% Al doped SnO_2 thin films. This behavior is not expected for doped transparent conducting oxides. For the undoped and low Al doped films, the optical constants are qualitatively different. In this case k(λ) increases for increasing λ, as expected for a metallic material, while n(λ) drops gently towards larger λ. These effects decrease in magnitude with increasing doping level of Nb.

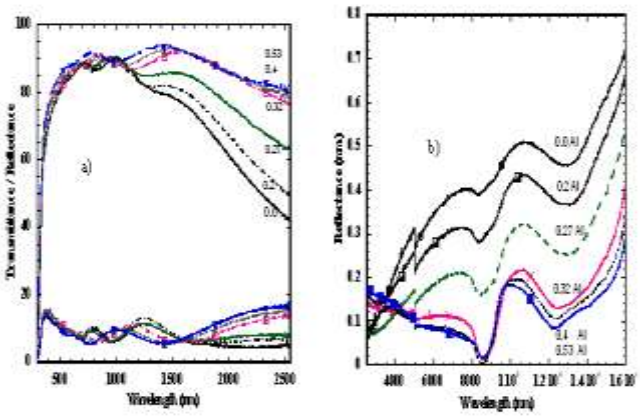

Fig. 7(a) Experimental Spectral Transmittance and Reflectance of undoped and Al-doped tin oxide films films with a thickness of 309 nm in the wavelength range 300 to 2500nm (b) Experimental reflectance of undoped and Al-doped tin oxide films in the far infrared wavelength range.

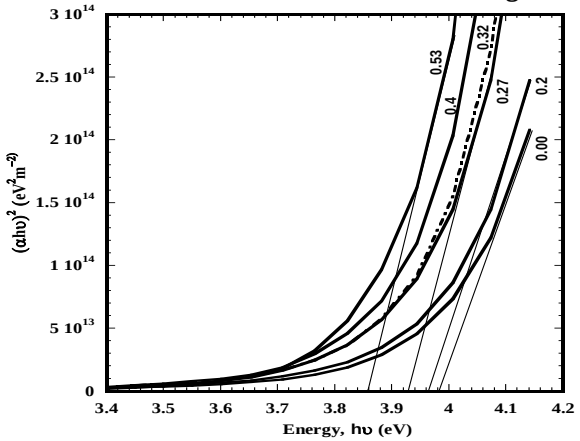

Fig. 8 $(\alpha h\nu)^2$ versus hv plots for determining the optical direct bandgaps of undoped and doped tin oxide films with various spray ratios $Alcl_3 : SnO_2$ as indicated in the figure

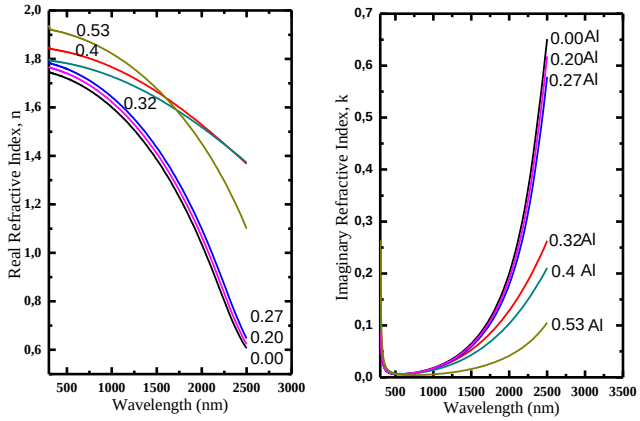

Fig. 9: Spectral refractive index and extinction coefficient for SnO_2 and $SnO_2 : Al$ films after annealing in 1 atm H_2 atmosphere at 500˚C for 1 hour

Figure 9 also shows that there is no significant difference in the optical properties with Al doping. The optical modeling results show a decrease of the carrier concentration with Al doping. This is in accordance with the valence control principle [17]. The valence control principle predicts that when trivalent ions (Al^{3+}) are partially introduced into the lattice, the carrier concentration, n, of SnO_2 will be reduced, leading to an increase in Debye length [17].

Discussion

Our main aim was to fabricate a p-type material. Possible reasons for failure to obtain a p-type material is outlined below. To achieve p-type conductivity, a material having a relatively low work function is required. This is a challenge for metal oxide systems such as tin oxide since most are characterized by relatively large work functions due to the nature of the metal – oxygen bond [20]. Another reason may be due to defect stability as a function of defect concentration. As more defects are added to a lattice in substitutional positions, the lattice can be prone to destabilization, possibly resulting in phase segregation[20]. This is promoted by disperities in cation (anion) dopant sizes with respect to those comprising the base material. As the lattice distorts, the possibility for forming killer defects also will increase. Killer formation is a response of the system to resist further insult to its structure and bonding arrangement [20]. The difficulty in producing p-type TCO's appears to be related to the strong localization of O 2p states, that form the upper edge of the valence band.

Conclusion

Conducting and transparent thin films of Al doped SnO_2 glass substrates were successfully synthesized at 480^{o}C by the low cost, vacuum-free spray pyrolysis. We have demonstrated that Al doping lowers the grain size and conductivity of tin oxide films. All the prepared films turned out to be n-type judging from hot point probe measurements.

Acknowledgements

The authors would like to thank the International Program in the Physical Sciences (IPPS), Uppsala University. for the financial and material support to the Department of Physics, Moi University.

References

1. Karlson T., Roos A. and Ribbing C. G. Solar Energy Materials 11 (1985) 469 – 487
2. Chopra K. L., Major S. and Pandya D. K. Thin Solid Films, 102 (1983) 1 – 46
3. Chacko S., Philip N. S., and Vaidyan V. K. Phys. Stat. Sol. (a) 204, No. 10, 3305 – 3305 (2007)
4. Mohammad-Mehdi B. and Mehrdad S., J. Phys.D: Appl. Phys 37 (2004) 1248-1253
5. Peng C. H. and Desu S. B., J. Am. Ceram. Soc. 77, 929 (1994)
6. Hartridge A., Krishna M. G. and Bhattacharya, J. Phys. Chem. Solids 59(6/7), 859 (1998)
7. Swanepoel R. J. Phys. E, Sci. Instrum. 16, 1214 (1983)
8. R. F. Pierret, Semiconductor Device Fundamentals. Addison-Wesley, 1996.
9. Quadri S. B., Skelton E. F., Hsu D., Dinsmore A. D., Yang Y., Gray H. F., Ratna B. R., Phys. Rev. B 60, 9191 (1999)
10. John B. Mooney and Shirley B. Radding, Ann. Rev. Mater. Sci. 1982. 12:81-101
11. K. Von Rottkay, M. Rubin Mater. Res. Soc. Symp. Proc., 426, (1996) 449
12. Mwamburi M.,anders H., Ewa Wackelgård, Sol. Energ. Mat. & sol. cells 84 (2004) 381-394.
13. Poupon L., Iacconia P. and Pijolat C., Journal of the European Ceramic Society 19 (1999) 747-751
14. Jain K., Pant R. P., Sensors and Actuators B 113 (2006) 823–829
15. Sk. F. Ahmed · S. Khan · P. K. Ghosh · M. K. Mitra ·K. K. Chattopadhyay; Sol-Gel Sci Techn (2006) 39:241–247

16. Sk.F. Ahmed, P.K. Ghosh, S. Khan, M.K. Mitra, K.K. Chattopadhyay; Appl. Phys. A 86, 139–143 (2007)
17. Xu C., Tamaki J.,Miura N., and Yamazoe N., Talanta, Vol. 38, No. 10 pp 1169 – 1175 (1991)
18. W. Q. Hong, J. Phys. D: Phys. 22, 1384-1385, 1989
19. Summitt R., Marley J., and Borrelli N., J. Phys. Chem. Solids 25, 1465-1469, 1964
20. Exarhos G. J., Xiao-Dong Z., thin solid films , 515, (2007) 7025-7052
21. Gordon R.G., MRS Bulletin Pg 52 -57 August 2000
22. G. Sanon, A. Rajrup, Mansingh, Thin Solid Films 190 (1990) 287.
23. B.S. Chiou, S.T. Hsieh, W.F. Wu, J. Am Ceram. Soc. 77 (1994) 1740.
24. I.S. Mulla, H.S. Soni, V.J. Rao, A.P.B. Sinha, J. Mater. Sci. 21 (1986) 1280.
25. Y. Takahashi, Y. Wade, J. Eletrochem. Soc. 127 (1990) 267.
26. R. Alcantara, F. J. Fernandez-Madrigal, C. Perez-Vicente, J. L. Tirado,
J. Claude Jumas, and Josette Olivier-Fourcade ; Chem. Mater. 2000, 12, 3044-3051
27. Cabezas M.D.; Lamas D.G.; Baby R.E.; 4Cabanillas E.; Walsöe de Reca N.E.; The Journal of the Argentine Chemical Society ISSN 0365-0375 versión impresa